ACS OMEGA

http://pubs.acs.org/journal/acsodf

Article

Graphene-Reinforced Zn−Ni Alloy Composite Coating on Iron Substrates by Pulsed Reverse Electrodeposition and Its High Corrosion Resistance

Sishi Li, Gongsheng Song, Yupeng Zhang,* Qiang Fu, and Chunxu Pan*

Cite This: *ACS Omega* 2021, 6, 13728−13741

Read Online

ACCESS | Metrics & More | Article Recommendations | Supporting Information

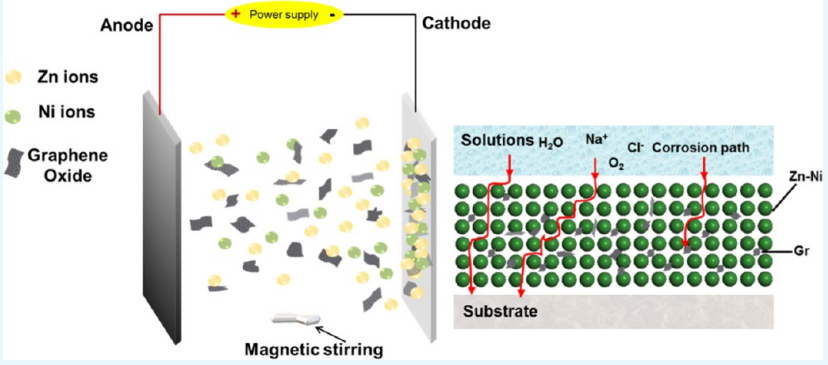

ABSTRACT: In this paper, a novel kind of graphene (Gr)-reinforced Zn−Ni alloy composite coating is successfully prepared on an iron substrate by pulsed reverse electrodeposition. Hydrophilic graphene oxide (GO) is directly added to the electrolyte and reduced to Gr during coating. The experimental results reveal that (1) there is an optimal adding amount (about 0.4 g/L) of GO in the electrolyte for achieving the highest mechanical properties and corrosion resistance; (2) the composite coating shows grain refinement and a dense microstructure due to heterogeneous nucleation sites provided from the Gr sheets during electrodeposition; and (3) compared to the regular Zn−Ni coating, the composite coating exhibits many enhancements, including hardness increase by 2.3 times, elastic modulus increase by 39%, and corrosion rate decrease from 37.66 to 1.30 mils/annum. This process has advantages such as being simple, effective, well repeatable, economical, and supporting large-scale production and is expected to be widely applied in electronics, automobiles, marine engineering, and military industries.

1. INTRODUCTION

It is well known that Zinc (Zn) and Zn-based alloy coatings, involving zinc−cobalt (Zn−Co), zinc−nickel (Zn−Ni), zinc−chromium (Zn−Cr), zinc−copper (Zn−Cu), and zinc−iron (Zn−Fe), provide economical ways to enhance the anti-corrosion performance of iron and steel, which has been employed in industry widely.[1−7] In recent years, in order to enhance the corrosion resistance of thin coatings in harsh environments, many composite coatings have been developed for meeting challenging applications.[8,9] As we all know, compared with their bulk materials, nano-sized materials have a significant large surface area to volume ratio and therefore, nanocomposite coatings have been widely explored for applications.[10] Correspondingly, various nanomaterials have been used as reinforcing phases for preparing the composite coatings in the field of electrodeposition, such as zinc−nickel alloy−cerium oxide (Zn−Ni alloy−CeO_2), zinc−nickel alloy−aluminum oxide (Zn−Ni alloy−Al_2O_3), zinc−nickel alloy−silicon nitride (Zn−Ni alloy−Si_3N_4), zinc−titanium oxide (Zn−TiO_2), zinc−nickel−phosphorus alloy−silicon carbide (Zn−Ni−P alloy−SiC), nickel−phosphorus alloy−tungsten carbide (Ni−P alloy−WC), zinc−nickel alloy−carbon nanotubes (Zn−Ni alloy−CNTs), nickel−reduced graphene oxide (Ni−rGO), and zinc−graphene (Zn−Gr).[11−23]

As a novel two-dimensional material, graphene (Gr) has been considered as an ideal reinforcing phase in composites due to its unique properties, such as excellent thermal conductivity (3000−5000 W m^{-1} K^{-1}), large theoretical specific surface area (2630 m^2 g^{-1}), excellent mechanical properties, remarkable chemical inertness unless exposed to harsh reaction conditions, and so forth.[24−26] So far, various metal/alloy−Gr composites, such as iron (Fe), copper (Cu),

Received: February 23, 2021
Accepted: May 6, 2021
Published: May 17, 2021

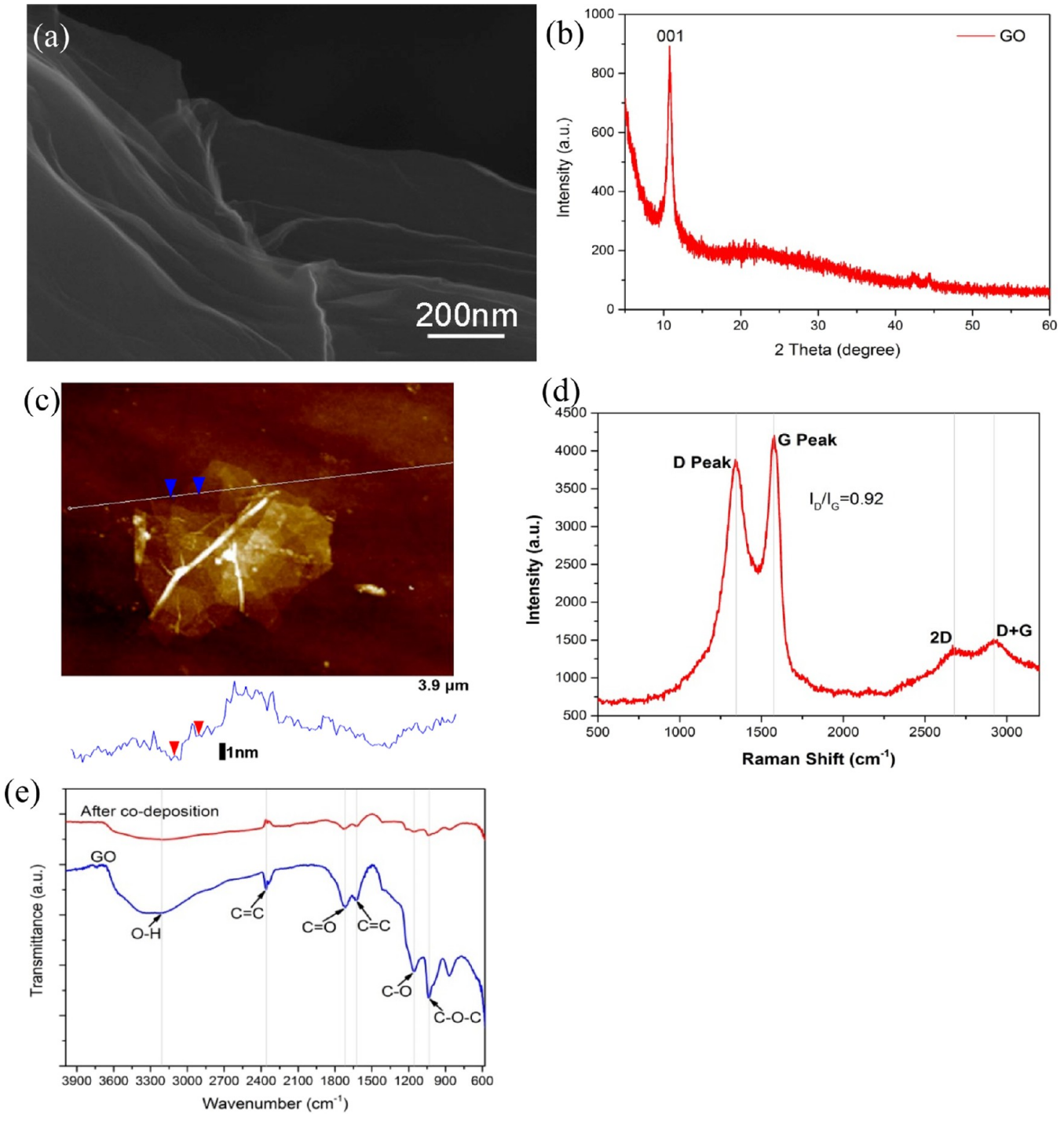

Figure 1. Characterizations of GO: (a) SEM morphology; (b) XRD pattern; (c) AFM image; (d) Raman spectrum; and (e) FT-IR spectra before and after co-deposition.

nickel (Ni), aluminum (Al), gold (Au), silver (Ag), and so forth, have been prepared by using different processes including electrochemical deposition and powder metallurgy.[27−33] Zhang et al.[29] prepared the Fe−Gr composite coating on the copper substrate coupled with aluminum by the electroless plating process. Luo et al.[30] employed the Ag−Gr as a reinforcing phase to prepare the copper matrix composites via ball milling and hot-pressed sintering at different pressures, and the micro-hardness and electrical and thermal conductivities were all higher than pure copper. Leng et al.[31] fabricated the Al−Gr composite by the powder metallurgic method and the hardness increased by 33.5%. Rekha et al.[4] performed the ZnCr−graphene oxide (ZnCr−GO) composite coatings over a mild steel substrate by using electrolyte baths with different concentrations of dispersed GO and revealed that for both 1 and 48 h exposure times, the composite coatings were of higher corrosion resistance than the ZnCr coatings, and the corrosion resistance substantially increased with GO content increase during coatings. Jabbar et al.[32] fabricated the Ni−Gr composite coatings on carbon steel at different deposition temperatures, and the results showed that the coating deposited at 45 °C exhibited a coarser surface morphology

https://doi.org/10.1021/acsomega.1c00977
ACS Omega 2021, 6, 13728−13741

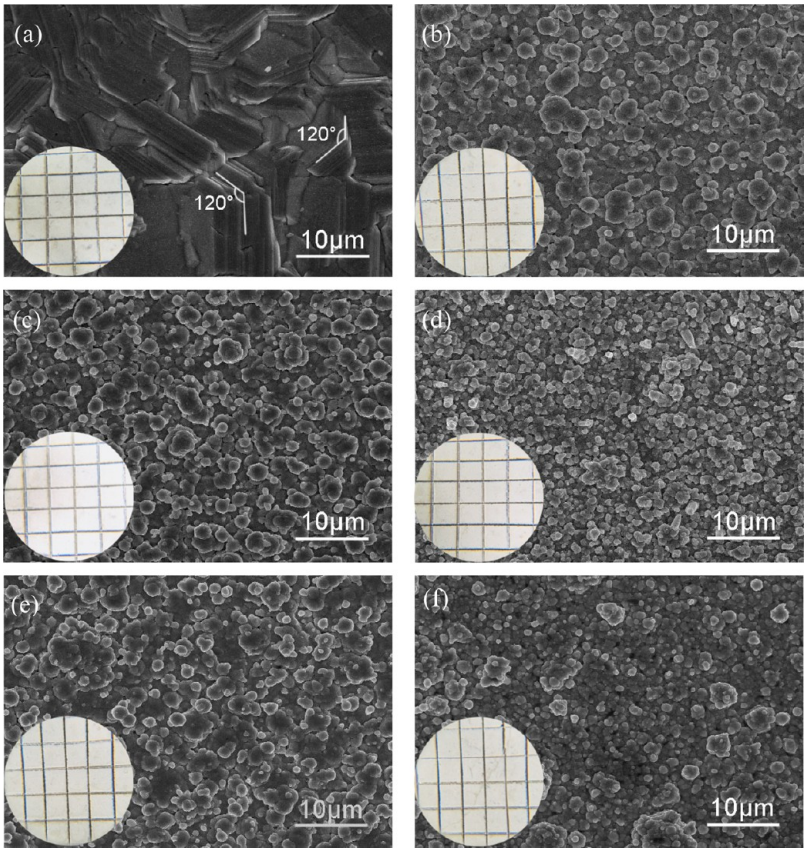

Figure 2. Surface SEM morphologies of the coatings: (a) pure Zn; (b) regular Zn−Ni alloy; (c−f) Zn−Ni alloy−Gr with different GO contents in the electrolyte from 0.2, 0.4, 0.6 to 0.8 g/L, respectively. The inset is the surface morphologies of the coatings after the cross-cut tape testing.

with increased carbon content, refined grain sizes, high micro hardness, and better corrosion resistance performance. In our previous work, the Cu−Gr composite coating via electroless plating[33] and the Fe−Gr[27] and Zn−Gr[19] composite coatings via electrodeposition were prepared, which showed enhanced mechanical property and corrosion resistance. In addition, the Cu−Gr composite based upon high-quality graphene was also prepared via spark plasma sintering and exhibited better electrical conductivity.[34]

Electrodeposition is a technique that holds great promise for large-scale applications of metal−Gr composite coatings with easy processing and low cost. In general, graphene (Gr) has poor dispersibility in water. However, as a kind of oxidized form of Gr, GO not only exhibits relatively good barrier and mechanical properties but also has many hydrophilic functional groups, such as the hydroxyl group, epoxy group, and carboxyl group, which can easily form hydrogen bonds with water molecules and provides a possibility to achieve uniform dispersion in the electroplating solution.[35−37] In this work, the Zn−Ni alloy−Gr composite coating was prepared by using pulsed-reverse electrodeposition (PRED). PRED is a simple and economical process for depositing porosity-free, bulk nanocrystalline materials with controlled physical properties and exhibits better corrosion resistance than conventionally deposited metal coatings.[38] Instead of hydrophobic Gr, hydrophilic GO was added in the electrolyte bath and reduced to Gr during the co-deposition process. The Gr-reinforced Zn−Ni alloy coating achieved great improvement of mechanical property and corrosion resistance at the optimum adding amount of GO. The process has advantages such as being simple, effective, well repeatable, economical, and promoting large-size production and is expected to be widely applied in electronics, automobile, chemical, marine engineering, and military industries.

2. RESULTS AND DISCUSSION

Figure 1 shows the microstructures of GO. Obviously, GO exhibited thin and transparent sheets with irregular shapes, which indicated that natural graphite had been peeled off into single and few-layered sheets of about 1 nm after oxidation and ultrasonic treatment. Meanwhile, some folds were observed at the edge of the GO sheets due to destruction of the C═C bands, when it attached the oxygen-containing functional groups. The XRD pattern revealed an obvious carbon diffraction peak (110) at 10.9°, which was the characteristic absorption peak of GO, indicating its high degree of graphite oxidization and exhibiting an ordered crystalline phase.[37,39,40] In addition, because of the existence of the oxygen functional groups and water molecules in between the interlayer galleries of the hydrophilic GO, the interlayer spacing was enlarged up to 0.81 nm, which was much larger than that of the regular graphite interlayer (0.34 nm). From the Raman spectrum, a typical D band appeared at 1340.8 cm^{-1} corresponding to the irregular arrangement of atomics and the edge effects of Gr and a G band at 1578.7 cm^{-1} representing the plate vibrations of sp^2 carbon atoms. The ratio of I_D to I_G (I_D/I_G) was 0.92, which showed the typical spectra of GO.[41]

The FT-IR spectra illustrate more information on GO before and after electrodeposition. For original GO, the peaks related to different groups, that is, a broad peak at 3220.04

https://doi.org/10.1021/acsomega.1c00977
ACS Omega 2021, 6, 13728−13741

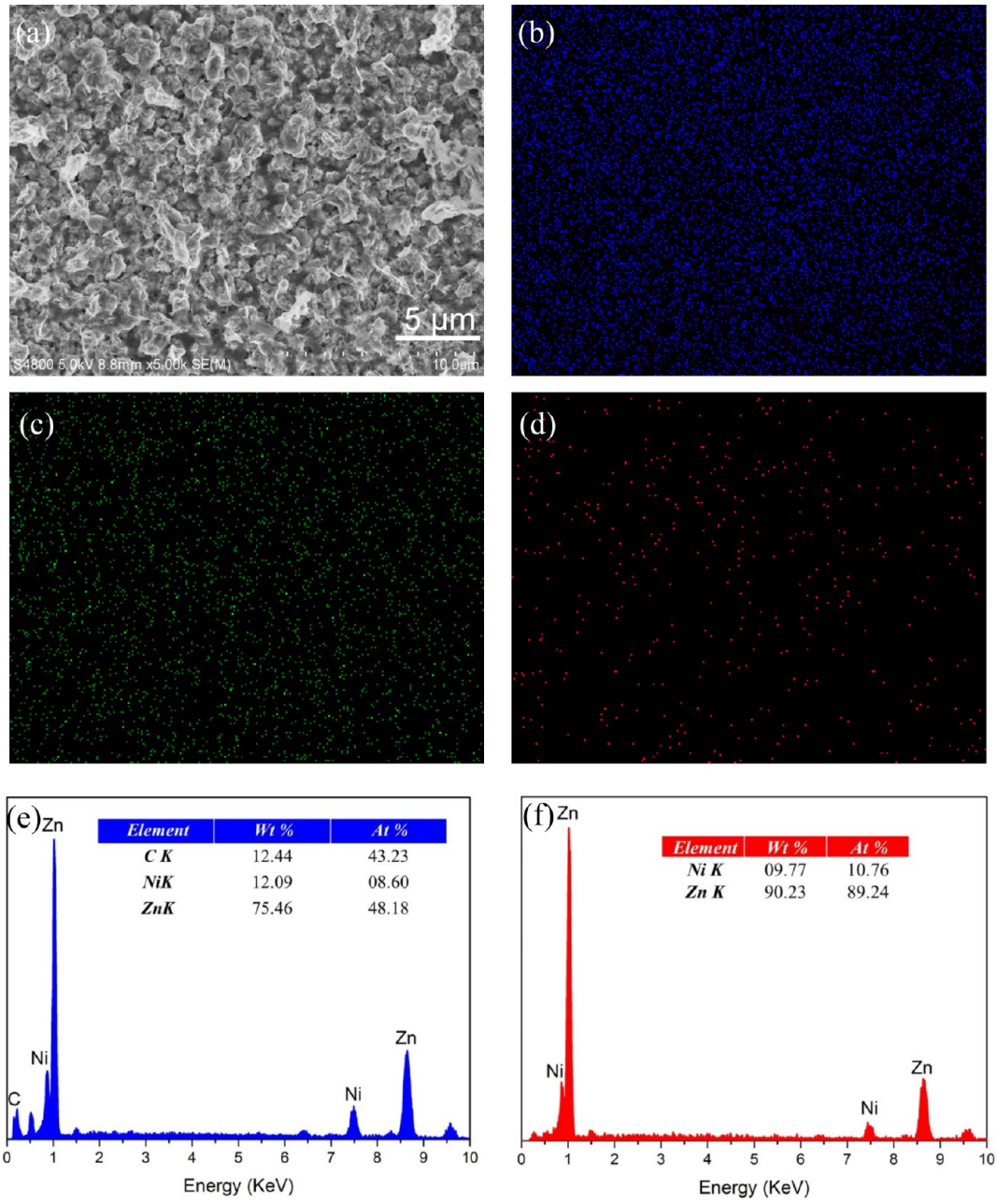

Figure 3. EDS elemental analysis of the coating's surface: (a) SEM image; (b–d) EDS mappings; (e) Compositions of the Zn–Ni alloy–Gr composite; and (f) Compositions of the regular Zn–Ni alloy.

cm^{-1} corresponding to O–H of the carboxyl group, the peak at 1716.57 cm^{-1} to C═O vibration of the carboxyl group or carbonyl group, the peak at 1624.44 cm^{-1} to C═C tensile vibration of the aromatic ring, and the peak at 1045.27 cm^{-1} to C–O vibration of carboxylic acid. Apparently, the existence of various active oxygen-containing groups (carboxylic groups at the edges and hydroxyl groups within the plates) on the internal and external surfaces confirmed the presence of GO, which was consistent with the reported results.[40] In addition, it also affected the surface polarity and changed the surface charge distribution, which further provided a possibility of the GO uniform distribution in the electrolyte and promoted the formation of even composite coating as discussed above.[42]

However, after the pulsed-reverse electrochemical deposition, it was worth especially to note that the peak related to the vibration of the C=O bond became smaller and narrower, and the absorption peaks of O–H stretching vibration almost disappeared. In addition, due to the tensile vibration of C–O and epoxy groups, the peak at 1153 cm^{-1} became very small. These results demonstrated that the most of the oxygen-containing groups have been removed from the carbon sheets during co-electrodeposition, and that was to say, GO sheets have been reduced and transformed into rGO or Gr effectively after electrochemical treatment.

In general, the reduction of GO is mainly caused by electronic exchange between GO and the electrodes.[43] In the present work, the larger cathode pulse is more beneficial to the GO reduction into Gr within the composite coating during electrodeposition. In addition, it was reported that the potential needed to achieve the reduction was controlled by

https://doi.org/10.1021/acsomega.1c00977
ACS Omega 2021, 6, 13728–13741

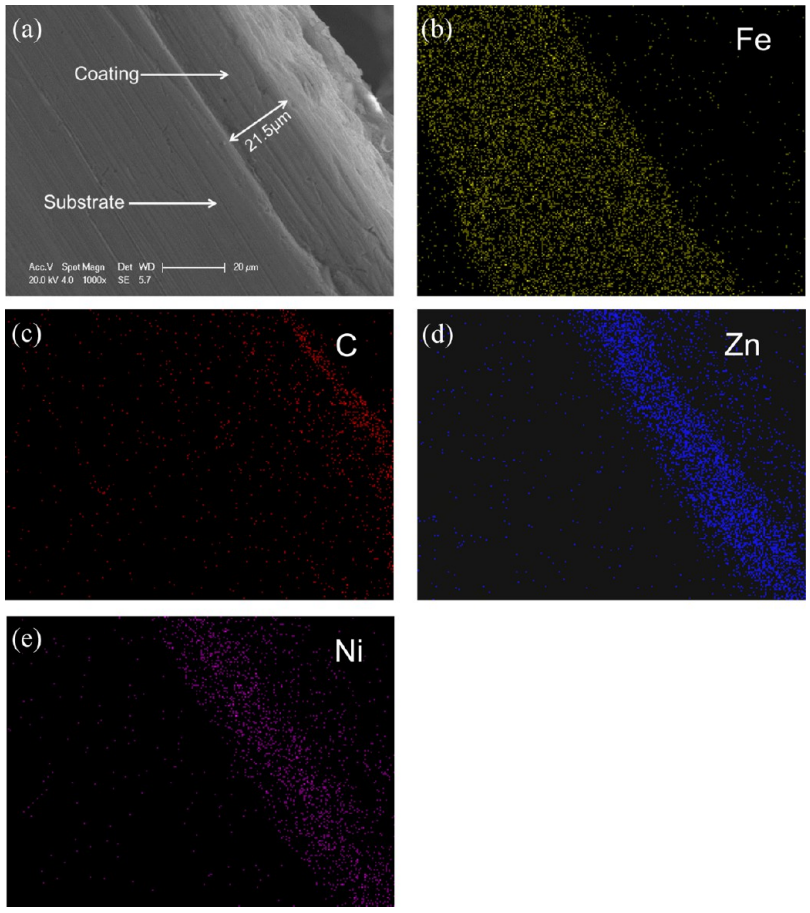

Figure 4. EDS elemental mappings of the cross section of the Zn−Ni alloy−Gr composite coating: (a) SEM; (b) Fe; (c) C; (d) Zn; and (e) Ni.

the pH value of the buffer solution. Hydrogen ions (H^+) participated in the reaction and the low pH value was favorable to GO reduction. The following equation highlights the crucial role of H^+ in the solution.[44]

$$\text{Graphene oxide} + a\text{H}^+ + be^- \rightarrow \text{reduced graphene oxide} + c\text{H}_2\text{O} \quad (4)$$

Figure 2 shows the surface morphologies of the coatings. It could be seen that the pure Zn coating exhibited a typical hexagonal close-packed structure; the Zn laminated crystalline grains grew in random orientations and stacked with each other at 120° edge angles. Comparatively, the regular Zn−Ni alloy coating showed great changes in crystallinity and morphologies, that is, the spherical nodules replaced the hexagonal clusters due to the formation of a new phase. Further, the grain sizes of the composite coating varied with the contents of the Gr-reinforcing phases, and the smallest and densest grains appeared at 0.4 g/L, as shown in Figure 2d. These results reveal three facts, that is, (1) the Gr sheets provided additional nucleation sites and resulted in small and dense grains, which changed the original homogeneous nucleation into heterogeneous nucleation during electrodeposition; (2) Gr also hindered the grain growth; (3) excessive GO sheets in the electrolyte decreased the content of the Gr-reinforcing phase in the coating due to agglomeration and poor dispersion and weakened the enhancement effect. In fact, the phenomenon of the "optimal Gr adding content" in the metal−Gr composites has been confirmed by many research studies.[19,27,37,45]

The inset shows the surface of the coatings after cross-cut tape testing. As we all know, the adhesion strength between the coating and the substrate is an important factor in practical applications. Clearly, the cut edges were smooth and none of the grid squares was detached from the substrate after stripping off the tape, which demonstrated a good adhesion between the coating and the substrate and had the highest value in accordance with the 5B level of the ASTM D3359 standard. All samples exhibited the same results, indicating that as a reinforcing phase, Gr did not make any obvious influences on appearance and adhesion strength of the coatings.

In general, it is difficult to directly measure the Gr distribution uniformity and content in the composites by instruments. Therefore, indirect methods, such as C elemental mapping and property variations, such as corrosion, hardness, tensile strength, and so forth are often used in experiments. Figure 3b−d shows the energy-dispersive X-ray spectroscopy (EDS) elemental mappings of the surface of the Zn−Ni alloy−Gr composite coating. Obviously, Zn, Ni, and C elements dispersed homogeneously in the coating without segregation and agglomeration. The C, Zn, and Ni compositions in the composite coating were 12.44, 12.09, and 75.46 wt %, respectively, which indicated the successful incorporation of Gr with Zn and Ni ions. From the cross-sectional image, as shown in Figure 4, the thickness of the coating was about 21.5 μm. The EDS elemental mappings, as shown in Figure 4b−e, further showed the uniform distribution of the elements in the

https://doi.org/10.1021/acsomega.1c00977
ACS Omega 2021, 6, 13728−13741

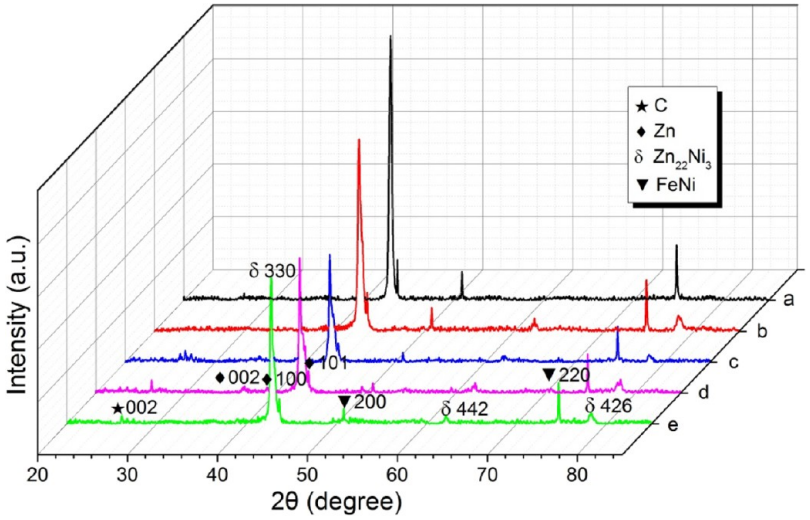

Figure 5. XRD patterns of the Zn−Ni alloy−Gr composite coatings with different GO contents added in the electrolyte: (a−e) 0, 0.2, 0.4, 0.6 to 0.8 g/L, respectively.

composite coating. Especially, the uniform dispersion of the C element could be ascribed to the homogeneous dispersion of GO in the electrolyte and dissolution effect at the current interruption (t_{off}) stage during deposition.

Figure 5 illustrates the XRD patterns of the samples. The peaks at 36.3, 39.1, and 43.2° corresponded to the (002), (100), and (101) crystal planes of metal Zn [PDF#87-0713]. The three peaks at 43, 62.1, and 78.2° can be ascribed to the (330), (442), and (426) crystal planes of the δ-phase (δ-$Zn_{22}Ni_3$) [PDF#10-0209], respectively. Comparatively, the peak width of the δ-phase (δ-$Zn_{22}Ni_3$) in the composite coating was broader than that of the regular Zn−Ni alloy coating, which revealed the smaller grain sizes due to the Gr co-deposition. According to the Scherrer equation, the calculated average crystal size of the coatings varied in the following sequence: 23.3, 17.9, 17.5, 18.4, and 19.4 nm, where the GO contents in the electrolyte were 0, 0.2, 0.4, 0.6, and 0.8 g/L, respectively. The variations were also consistent with the results in Figure 2. In addition, a very small peak at 26.1° was identified in the composite coatings, which was attributed to the diffraction of the (002) carbon planes.[39,46]

Corrosion resistance is crucial for applications of the protective coatings. In this work, first, electrochemical impedance spectroscopy (EIS) was applied to evaluate the corrosion property due to its capability of "in situ" and non-destructively probing relaxation phenomena over a wide range of frequencies. In order to obtain stable potentials with times, the equilibrium potential was measured by immersing the coated electrodes in a 3.5 wt % NaCl solution for 30 min before the corrosion measurement. As shown in Figure 6, the results indicated that: (1) the open circuit potential (E_{ocp}) value of the pure Zn coating shifted sharply to the negative direction at the beginning whereas that of the regular Zn−Ni alloy coating and the Zn−Ni alloy−Gr composite coatings decreased only by about 10 mV or even less with increase of immersion time; (2) the E_{ocp} values for the regular Zn−Ni alloy and the Zn−Ni alloy−Gr composite coatings (GO contents in the electrolyte: 0, 0.2, 0.4, 0.6, 0.8 g/L) were stabilizing at −1.074, −1.049, −1.039, −1.047, and −1.052 mV, respectively, which demonstrated that the Gr incorporation further reduced the corrosion susceptibility.

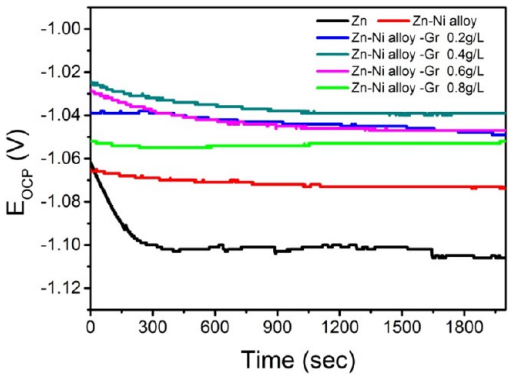

Figure 6. Open-circuit potential (E_{ocp}) curves in 3.5 wt % NaCl solution.

Figure 7 illustrates the EIS plots of the samples in 3.5 wt % NaCl aqueous solutions for 30 min. All Nyquist plots were of a similar shape, that is, two loops of different dimensions, one high-frequency capacitive loop, and one low-frequency capacitive loop. The equivalent circuit is used to explicate the corrosion resistance of the composite coating circuit. Figure 7d gives the electrical circuit, where R_s represents the solution resistance between the reference and working electrodes. R_o and CPE_3 correspond to the resistance and capacitance of the formation of the thin oxide film that is reinforced by the ionic conduction through its pores. The constant phase element, CPE, is used to replace the pure double layer capacitor and obtain a more accurate fit due to the distributed surface reactivity, roughness, and surface heterogeneity. R_c and CPE_2 correspond to the resistance and capacitance of the coatings. R_{ct} represents the charge transfer resistance, and CPE_1 corresponds to the electric double layer capacitance.[47] The related parameters derived from the models were summarized in Table 2. The charge-transfer resistances (R_{ct}) of the pure Zn and the Zn−Ni alloy coatings were 117.8 Ω cm^2 and 2677 Ω cm^2, respectively, whereas for the Zn−Ni alloy−Gr (0.4 g/L) coating, it reached up to 3815 Ω cm^2. It is well known that the low polarization resistance (R_{ct}) value is due to the increase of the active surface, which is related to the discontinuity and porosity of the coating, and the higher R_{ct}

https://doi.org/10.1021/acsomega.1c00977
ACS Omega 2021, 6, 13728−13741

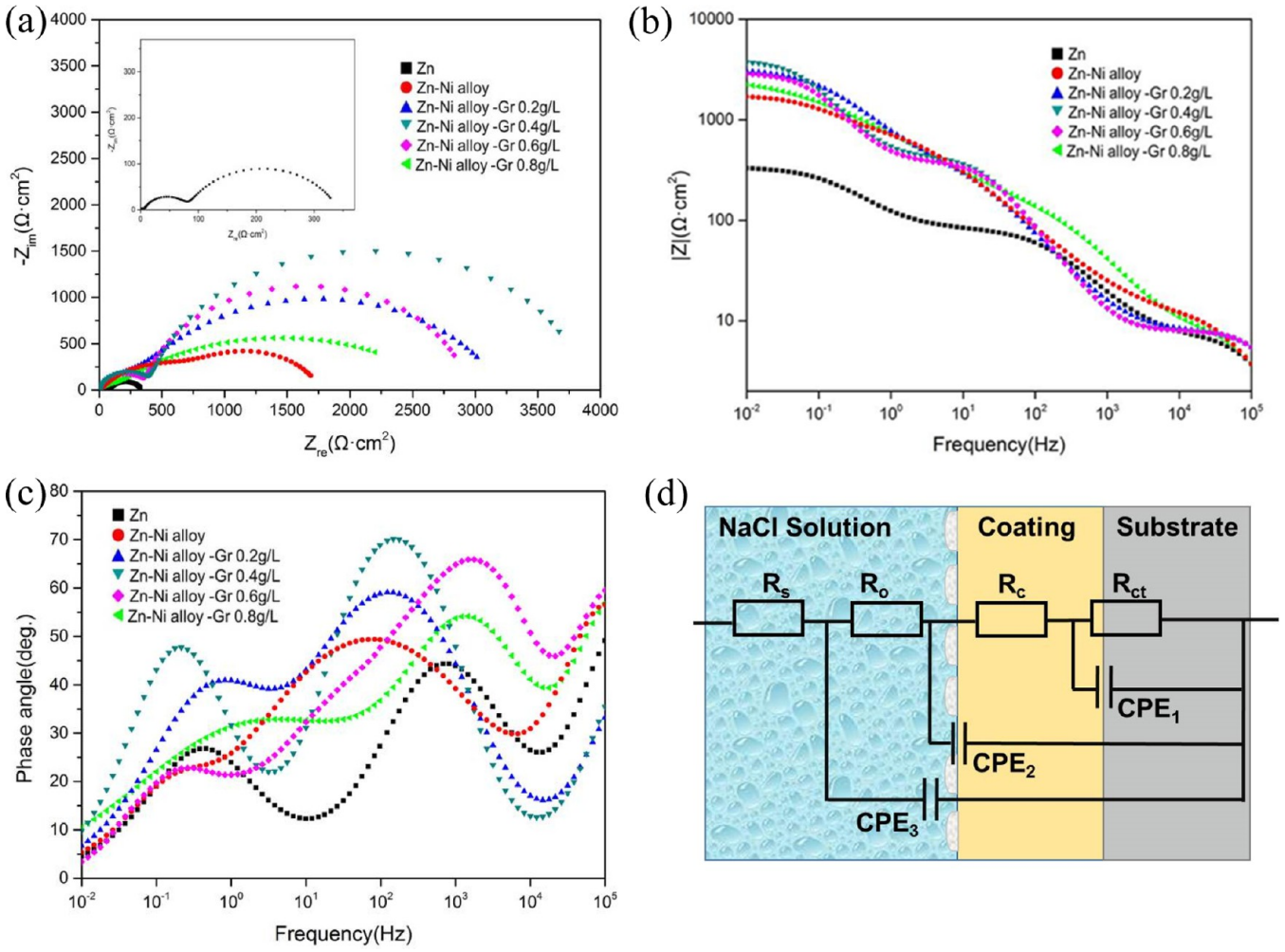

Figure 7. EIS plots of the samples in 3.5 wt % NaCl solution for 30 min: (a) Nyquist plots; (b) Bode |Z| versus frequency plots; (c) Bode—phase angle versus frequency plots; and (d) equivalent electrical circuits model used to fit the impedance spectra.

Table 1. Experimental Parameters of the Coating Preparations

compositions or parameters	pure Zn	Zn−Ni alloy	Zn−Ni alloy−Gr
nickel sulfate (g/L)	0	120	120
zinc chloride (g/L)	60	60	60
sodium sulfate (g/L)	80	80	80
SDS (g/L)	0.1	0.1	0.1
GO (g/L)	0	0	0.2, 0.4, 0.6, 0.8
pH	3.5	3.5	3.5
temperature (∘C)	40 ± 2	40 ± 2	40 ± 2
pulse frequency (Hz)	1000	1000	1000
duty cycle	50%	50%	50%
average current density (A/dm^2)	2	2	2
reverse average current density (A/dm^2)	0.5	0.5	0.5
deposition time (min)	10	10	10

value indicates better corrosion resistance. Therefore, these results demonstrated that the electrolyte was prevented to get into the composite coating, and meanwhile, the values of CPE_3 decreased for the Zn−Ni alloy−Gr composite coatings, which suggested that the passivating layer or corrosion layer became less permeable.[48]

With regard to Figure 7a, the Gr incorporation enlarged the dimension of the capacitive loop, implying an excellent corrosion resistance of the composite coating. The Bode modulus plot, as shown in Figure 7b, also showed that the maximum |Z| of the composite coating at the low-frequency range (f = 0.01 Hz) at the optimal GO concentration in the electrolyte was about twice higher than that of the regular Zn−Ni alloy coating. Similarly, the Bode phase plot, as shown in Figure 7c, revealed that the phase angle also increased after adding GO, which indicated that the presence of Gr changed the interface property between the metal and solution and effectively inhibited the corrosion of the substrate.[49,50]

Figure 8 illustrates the potentiodynamic polarization curves of the coatings in 3.5% NaCl solution and correspondingly, Table 3 lists the electrochemical parameters involving the corrosion current (i_{corr}), corrosion potential (E_{corr}), and linear polarization resistance (R_p) derived from the corrosion tests. These variations of i_{corr} and E_{corr} values indicated the high corrosion resistance of the composite coatings and furthermore, the minimum i_{corr} value occurred when the GO adding content was 0.4 g/L in the electrolyte. The corrosion rate (CR) (r_{corr}) could be calculated from i_{corr} by using Faraday's law of electrolysis[51]

https://doi.org/10.1021/acsomega.1c00977
ACS Omega 2021, 6, 13728−13741

Table 2. Calculation Values of the Equivalent Circuit Components of the Coatings in 3.5 wt % NaCl Aqueous Solution for 30 min

samples	R_s ($\Omega\cdot cm^2$)	CPE_3 ($F\cdot cm^{-2}$)	R_o ($\Omega\cdot cm^2$)	CPE2 ($F\cdot cm^{-2}$)	R_c ($\Omega\cdot cm^2$)	CPE_1 ($F\cdot cm^{-2}$)	R_{ct} ($\Omega\cdot cm^2$)
pure Zn	0.3226	3.23×10^{-7}	5.202	2.299×10^{-4}	94.49	8.561×10^{-3}	117.8
Zn−Ni alloy	0.7675	4.102×10^{-7}	8.697	1.363×10^{-5}	122	5.092×10^{-4}	2677
Zn−Ni alloy−Gr 0.2 g/L	1.981	2.91×10^{-7}	5.839	7.749×10^{-5}	469.2	3.664×10^{-4}	2261
Zn−Ni alloy−Gr 0.4 g/L	1.42	2.24×10^{-7}	7.652	2.163×10^{-4}	38.04	1.968×10^{-5}	3815
Zn−Ni alloy−Gr 0.6 g/L	1.629	2.753×10^{-7}	6.385	2.561×10^{-5}	384.4	7.422×10^{-4}	2552
Zn−Ni alloy−Gr 0.8 g/L	2.002	2.958×10^{-7}	5.923	7.555×10^{-5}	462.2	3.606×10^{-4}	2746

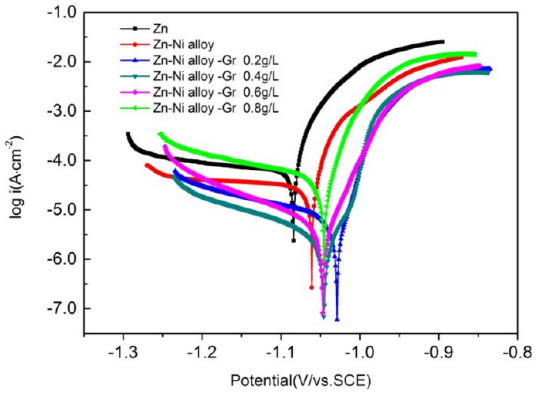

Figure 8. Potentiodynamic polarization curves of the samples in 3.5% NaCl solution.

$$r_{corr} = \frac{i_{corr} \times M}{Z \times F} t \quad (5)$$

where M is the atomic weight of the metal (56 g/mol for Zn), Z is the number of lost electrons per metal atom during the anodic dissolution of the metal, and F is the Faraday constant (96485.34 C/mol). The r_{corr} in this equation is the mass of dissolved metal in time per t unit area, which can be converted to corrosion depth by the following equation

$$CR = \frac{0.129 \times i_{corr} \times M}{Z \times \rho} \quad (6)$$

where ρ is the density of the metal undergoing corrosion (7.87 g/cm^3 for Fe) and "0.129" is the calculation parameter.[52]

Obviously, according to the CR values in Table 3, the corrosion resistance of the composite coatings was improved effectively due to the Gr incorporation. The mechanism could be explained as follows: (1) As an anode, Zn was dissolved and oxidized to Zn^{2+}, which was stable thermodynamically; (2) for the pure Zn coating, the corrosion products were mainly ZnO, while for the regular Zn−Ni alloy coating, the main corrosion products consisted of ZnO, $ZnCl_2\cdot Zn(OH)_2$ and a little of $2ZnCO_3\cdot 3Zn(OH)_2$;[53] (3) when the regular Zn−Ni alloy coating was in a corrosive environment, Zn was first corroded and produced white rust of $Zn(OH)_2\cdot 2H_2O$, which was a non-conductive substance and tended to form a dense $Zn(OH)_2$ film on the coating surface as a protective layer; (5) however, in the pure Zn coating, $Zn(OH)_2\cdot 2H_2O$ was easily converted into a ZnO film (a kind of n-type semiconductor) and formed a loosened film, and this film was in favor of passing through the corrosion current and weakened the shielding effect of the protective film; (6) the existence of the Ni element in the coating played a role in inhibiting the transformation from $Zn(OH)_2\cdot 2H_2O$ into the ZnO film and therefore, the Zn−Ni alloy coating held a smaller corrosion current and lower CR than the pure Zn coating; (7) more importantly, the well-dispersed Gr sheets in the composite coating acted as a barrier for preventing the penetration of corrosive media and further improved the corrosion resistance in corrosive environments; moreover, the best effect was acquired at the optimal GO adding content, about 0.4 g/L, in the electrolyte.

Figure 9 shows the surface morphologies of the coatings after immersing in 3.5 wt % NaCl solution for 30 min. Clearly, the pure Zn coating exhibited the worst corrosion surface, while regular the Zn−Ni alloy and the Zn−Ni alloy−Gr composite coatings were of much better corrosion resistance. Comparatively, in case the GO adding content was 0.4 g/L in the electrolyte, the composite coating showed the highest corrosion resistance, which was ascribed to the following three reasons: (1) the Gr-reinforcing phases provided more nucleation sites and retarded the grain growth, which resulted in the refined grain size and dense microstructures. In general, in nanostructured coatings, grain boundaries serve as suitable sites for nucleation and growth of the passivation layers. Therefore, in this work, a more stable and uniform passivation layer was formed and resulted in better corrosion resistance; (2) because of high impermeability, the Gr sheets exhibited barriers for preventing the penetration of the corrosion medium into the coating;[54] (3) the Gr-reinforcing phases entered and filled up with defects, such as cracks, gaps, crevices, and micro-scaled holes, generally generating in the metal matrix, which avoided the phenomenon of stress concentration and preferential corrosion. However, excessive addition of GO in the electrolyte would cause massive Gr agglomeration, resulting in insufficient Gr co-incorporation in the coating and reducing the corrosion resistance, as shown in Figure 9f.

Table 3. Electrochemical Parameters Derived from the Potentiodynamic Polarization Curves

sample	β_c ($V\cdot dec^{-1}$)	β_a ($V\cdot dec^{-1}$)	E_{corr} (V vs SCE)	i_{corr} ($uA\cdot cm^{-2}$)	R_p ($\Omega\cdot cm^2$)	CR mils/annum
pure Zn	1.769	10.043	−1.084	353.500	104	109.13
Zn−Ni alloy	0.753	11.439	−1.061	122.000	292	37.66
Zn−Ni alloy−Gr 0.2 g/L	3.309	12.068	−1.020	12.460	2269	3.85
Zn−Ni alloy−Gr 0.4 g/L	4.637	14.094	−1.046	4.199	5527	1.30
Zn−Ni alloy−Gr 0.6 g/L	5.827	18.389	−1.047	6.379	2815	1.97
Zn−Ni alloy−Gr 0.8 g/L	3.077	10.721	−1.046	92.110	342	28.43

https://doi.org/10.1021/acsomega.1c00977
ACS Omega 2021, 6, 13728−13741

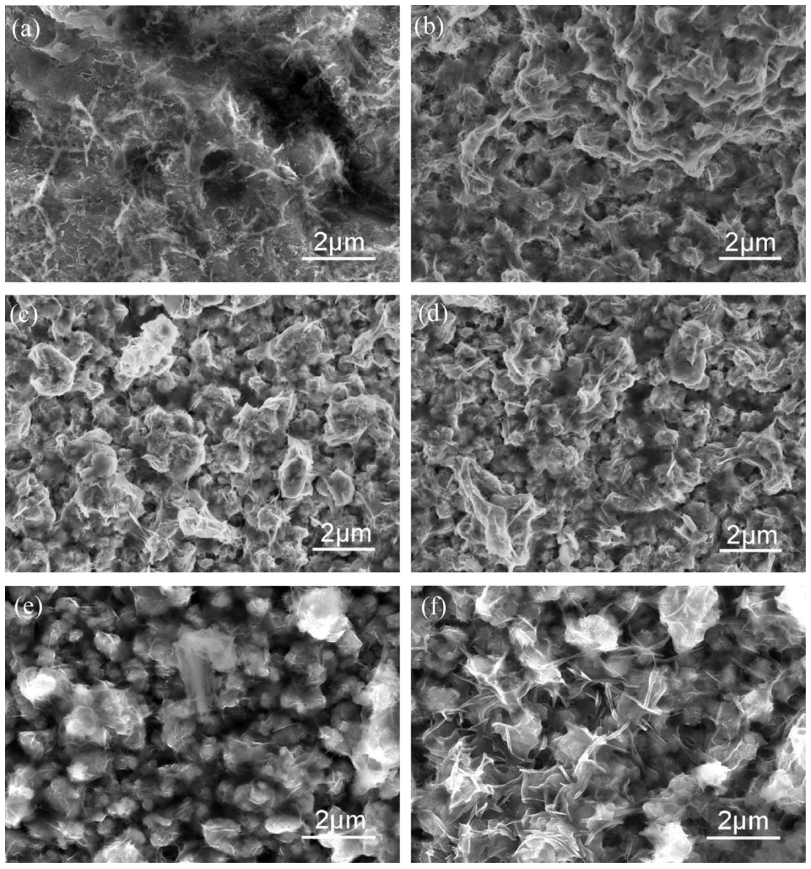

Figure 9. SEM surface morphologies of the samples after immersing in 3.5 wt % NaCl solution for 30 min: (a) pure Zn; (b) regular Zn−Ni alloy; (c)-(f) Zn−Ni alloy−Gr with different GO contents in the electrolyte from 0 to 0.8 g/L, respectively.

Figure 10 illustrates the coating cross section schematically. For the regular Zn−Ni coating, the substances Na^+, Cl^-, H_2O, O_2 in the corrosive solution were more likely to reach the substrate, as shown in Figure 10a, and it would suffer from corrosion easily. However, for the composite coating, the co-deposited Gr nanosheets acted as barriers in the corrosion paths and prevented the corrosive electrolyte from reaching the substrate, as shown in Figure 10b.

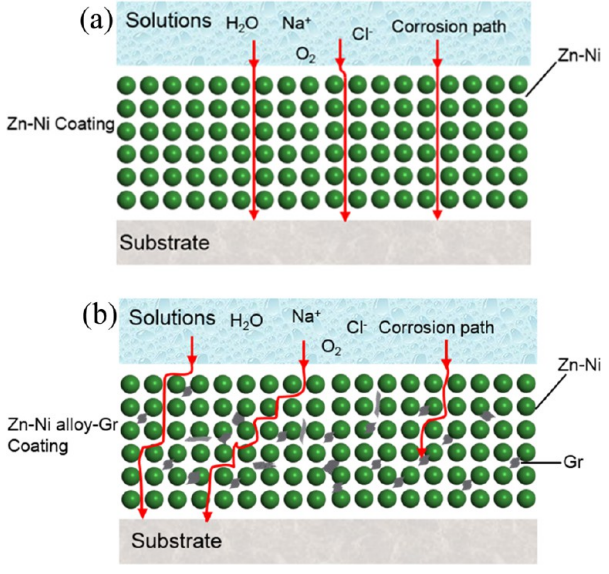

Figure 10. Schematic diagram of the coating cross section: (a) regular Zn−Ni alloy coating; (b) Zn−Ni alloy−Gr composite coating.

In order to investigate the corrosion-resistant perdurability of the coatings, Figure 11 shows the impedance spectra of the samples after immersing for 100 h in 3.5 wt % NaCl solution. Figure 11d gives the electrical circuit. The presence of an inductive loop suggested that the surface was not stable and the electrode process of the coating comprised the dissolution reaction involving adsorption/desorption of the intermediate. The corrosive electrolyte diffused through the defect site and reached the coating/metal interface, which led to the initiation of electrochemical reactions.[13] R_s was the solution resistance between the reference and working electrodes. R_c was the coating resistance and CPE_c represented the coating capacity, which characterized the medium capacitance loop and originated from the diffusion through the porous alloy surface. R_{ct} represented the charge-transfer resistance, which was ascribed to the redox reaction of the metal, and CEP_{dl} corresponded to the electric double layer capacitance, describing the low-frequency capacitive loop. R_L and L described the inductive loop, which corresponds to the resistance of intermediate adsorption/desorption and the inductance of Faradaic processed occurrence at the electrode. From Table 4, it could be seen that the values of R_{ct} had a significant increase for the Zn−Ni alloy−Gr composite coating ($368.4\Omega\cdot cm^2$) when compared to the pure Zn ($108.7\Omega\cdot cm^2$) and Zn−Ni alloy coating ($300.9\ \Omega\cdot cm^2$). Also, the values of CPE_c and CEP_{dl} were much smaller, implying an increase in corrosion resistance of the coatings after incorporating Gr due

https://doi.org/10.1021/acsomega.1c00977
ACS Omega 2021, 6, 13728−13741

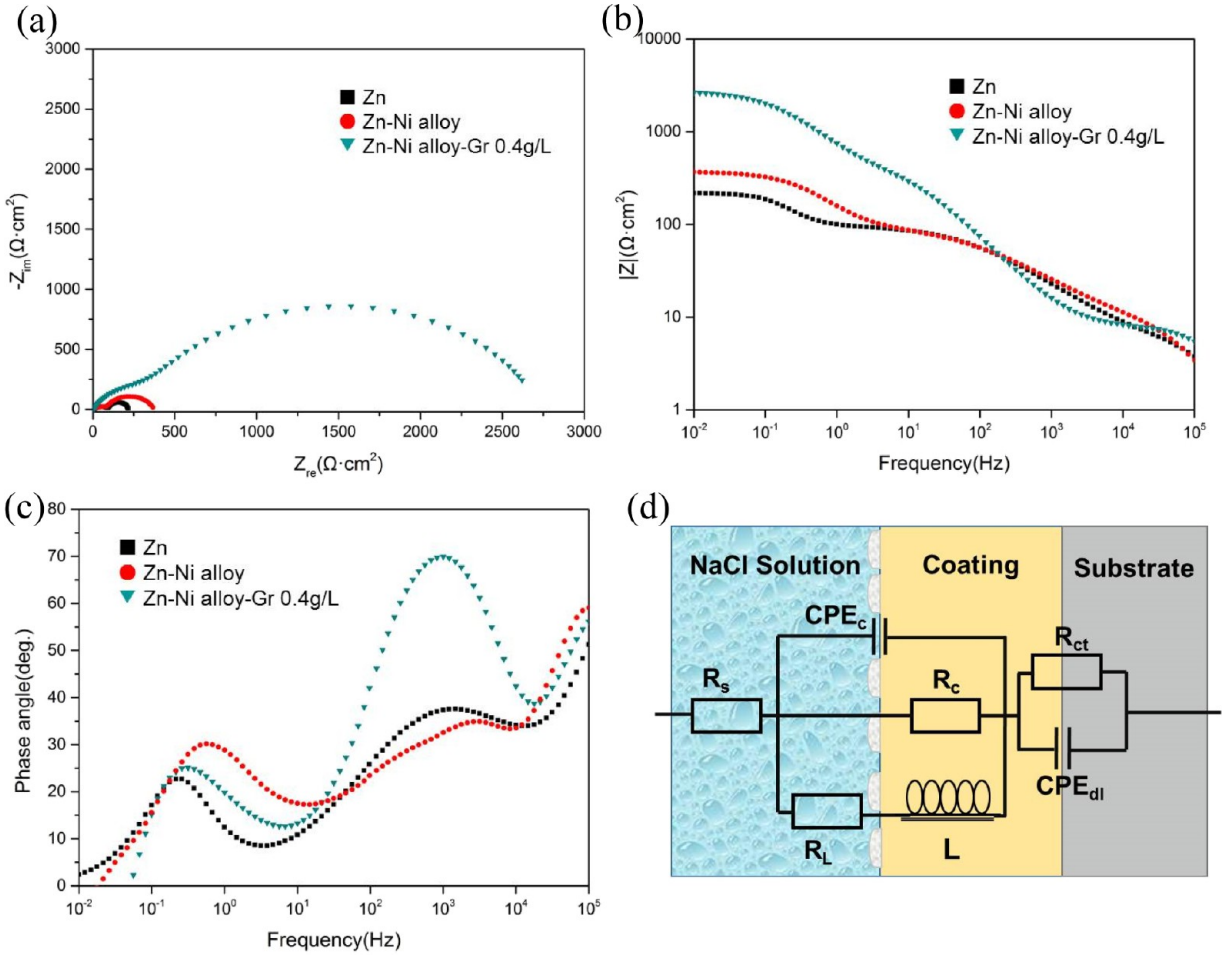

Figure 11. EIS plots of the samples in 3.5 wt % NaCl solution for 100 h: (a) Nyquist plots; (b) Bode |Z| versus frequency plots; (c) Bode—phase angle versus frequency plots; and (d) equivalent electrical circuits model used to fit the impedance spectra.

Table 4. Calculation Values of the Equivalent Circuit Components of the Coatings in 3.5 wt % NaCl Aqueous Solution for 100 h

samples	R_s ($\Omega \cdot cm^2$)	CPE_c ($F \cdot cm^{-2}$)	R_c ($\Omega \cdot cm^2$)	L (H)	R_L ($\Omega \cdot cm^2$)	CPE_{dl} ($F \cdot cm^{-2}$)	R_{ct} ($\Omega \cdot cm^2$)
pure Zn	2.274×10^{-4}	8.392×10^{-4}	164.2	6.825	339.3	1.018×10^{-2}	108.7
Zn−Ni alloy	1.908×10^{-6}	4.497×10^{-4}	96.13	1576	122	2.324×10^{-3}	300.9
Zn−Ni alloy−Gr 0.4 g/L	6.066	4.436×10^{-4}	3669	64050	7604	5.871×10^{-5}	368.4

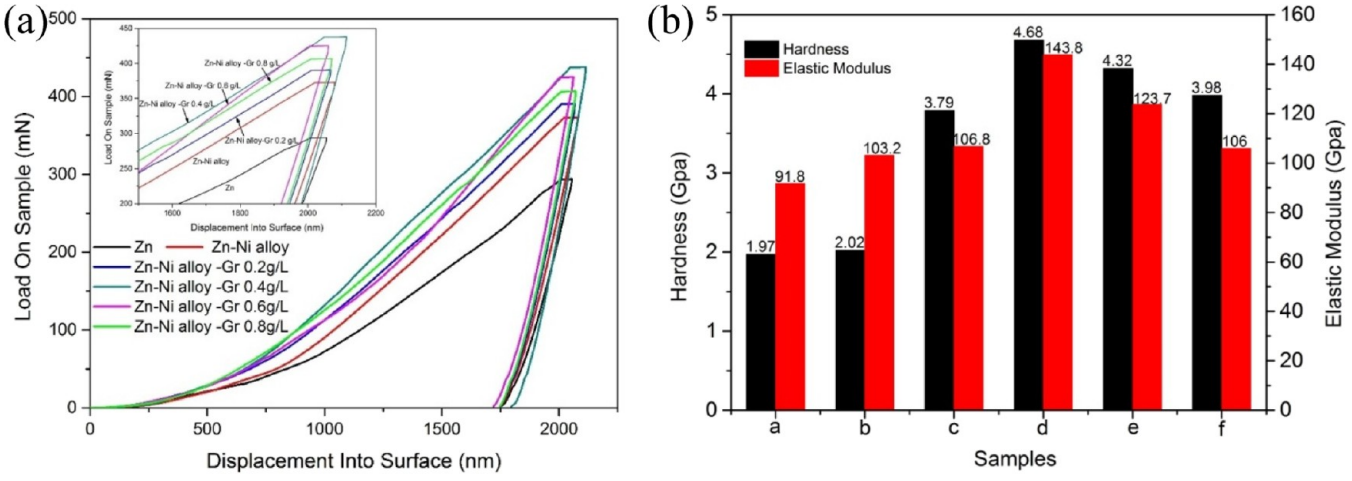

Figure 12. Mechanical properties of the samples: (a) load−displacement curves; (b) hardness and elastic modulus histograms (a−f: pure Zn, Zn−Ni alloy−Gr with different GO contents in the electrolyte 0, 0.2, 0.4, 0.6, and 0.8 g/L).

https://doi.org/10.1021/acsomega.1c00977
ACS Omega 2021, 6, 13728−13741

to the change of the microstructure and the formation of a compact passive layer or corrosion product layers.

Compared with Figure 7, the plots shrink to a smaller dimension. It indicated that the electrolyte diffused into the coating/metal interface through the coating porosities and defect sites and resulted in a decrease of the corrosion protection performance. As shown in Figure 11, the |Z| value of the Zn−Ni alloy−Gr composite coating was much larger than that of pure Zn and Zn−Ni alloy coatings. It suggested that the performance of the composite coating was stable and the rate of performance degradation was slower than the others. That was to say, the impermeability of the Gr sheets within the composite coating could effectively inhibit the ions' transport for a long time. Figure S2 illustrates the weight loss profiles of the coatings immersed in 3.5 wt % NaCl solution for 30 days. Obviously, the losses in the mass of the pure Zn and regular Zn−Ni alloy coatings were much higher than that of the Zn−Ni alloy−Gr composite coatings. Comparatively, in case the added GO content was 0.4 g/L in the electrolyte, the mass loss rate was the lowest, indicating the highest corrosion resistance, consistent with the results of the above electrochemical tests.

The mechanical properties of the coatings are also very important in engineering applications. Figure 12 gives the load−displacement curves, hardness, and elastic modulus of the coatings measured by using a nanoindenter. It could be seen that at the optimal adding content of GO, the microhardness of the Zn−Ni alloy−Gr composite coating increased to 4.68 GPa whereas those of the pure Zn and regular Zn−Ni alloy coatings were only 1.97 and 2.02 GPa, respectively. Meanwhile, the elastic modulus also increases by 39 and 57%, respectively. The enhancement of Gr on the mechanical properties of the composite coatings was also examined by many other research studies.[11,21,22,33,37] These enhancement mechanisms were ascribed as follows: (1) the Zn−Ni alloy was similar to a metallic solid solution and Ni atoms replaced part of lattice sites of Zn atoms, which resulted in the atomic lattice distortion and hindered the deformation caused by an external force; (2) the Gr-reinforcing phase in the coating increased the nucleation sites for the reduction of metal ions and hindered the grain growth, which resulted in the refinement of grain size and a dense microstructure; (3) the strengthening effects of Gr also included the inhibition of plastic flow due to blocking of the dislocation motion, grain refinement, and inherent high mechanical strength of Gr itself.

3. CONCLUSIONS

1) The Gr-reinforced Zn−Ni alloy composite coating is successfully prepared by PRED. During preparation, hydrophilic GO is added in the electrolyte and reduced into Gr and also co-deposited with Zn and Ni ions.
2) The Gr-reinforcing phase in the coating increases the nucleation sites for the reduction of metal ions and hindered the grain growth, which results in the refinement of grain size and a dense microstructure.
3) There exists an optimal GO adding content (0.4 g/L) in the electrolyte for achieving the highest performance. Compared to the regular Zn−Ni coating, the composite coating is of increased hardness by 2.3 times, elastic modulus by 39%, and decreased CR from 71.64 to 2.47 mils/annum.
4) The present process has advantages, such as easy and simple operation, excellent performance, and being suitable for industrial manufacture. It is expected to have broad application prospects in the fields of corrosion resistance, chemical engineering, military industry, marine engineering, aerospace, and so forth.

4. EXPERIMENTAL PROCEDURE

All reagents in this experiment were of analytical grade, and deionized water was utilized to prepare the electrolyte.

4.1. Preparation of Hydrophilic GO. Hydrophilic GO was synthesized from natural graphite by the modified Hummers method.[55] The preparation steps were as follows:

1) Pretreatment of graphite powder: 10 g of graphite powder (C), 10 g of potassium thiosulfate ($K_2S_2O_3$), and 10 g of phosphorus pentoxide (P_2O_5) were put into 15 mL of concentrated sulfuric acid (98% H_2SO_4) and then stirred for 6 h in a water bath at 80 °C. At last, the obtained dark mixture was filtrated by deionized water several times and dried in a stove at 60 °C;
2) Oxidation of graphite: First, 1 g of pretreated graphite was put into 30 mL of concentrated sulfuric acid (98% H_2SO_4), and 4 g of potassium permanganate ($KMnO_4$) was gradually added into the solution with stirring and cooling with an ice-water bath (<10 °C); Second, the solution was kept in a water bath at 35 °C for 2 h. Eventually, a dark tan solution was obtained after 30 mL of deionized water was added to the solution and kept at 85 °C for 30 min;
3) Hydrogen peroxide (30% H_2O_2), which was used to eliminate the excess potassium permanganate ($KMnO_4$), was slowly added until there were no bubbles in the solution and the color of the mixture turned into bright yellow;
4) Cleaning: the filtered product was washed twice in 10% diluted hydrochloric acid (5 mL of HCl + 45 mL of deionized water) and then rewashed 2−3 times in deionized water and alcohol;
5) Finally, hydrophilic GO was obtained after filtering, drying, and heating in a furnace at 30−50 °C for 24 h.

4.2. Preparation of the Zn−Ni Alloy−Gr Composite Coatings. The coatings were prepared on the Fe substrates via PRED with the following parameters,[56] that is, duty cycle (θ) is defined with respect to the ratio of power on time to total time in a pulse cycle, as shown in eq 1; frequency (f) is defined as the number of cycles per unit time and obtained by eq 2; and average current density (i_{ave}) is the total passed current divided by the total deposition time, which is related to peak current density according to eq 3. Figure S1a and Table 1 illustrate the schematic shape of the applied PRED and relevant key conditions.

$$\theta = \frac{t_{on}}{t_{on} + t_{off}} \quad (1)$$

$$f = \frac{1}{t_{on} + t_{off}} \times 100 \quad (2)$$

$$i_{ave} = i_p \times \theta \quad (3)$$

In general, during electrodeposition, the reinforcing phase can be co-deposited into coating by a number of processes, including convection of the reinforcing phase toward the cathode surface, mechanical entrapment of the reinforcing phase into the growing metal matrix, and electrophoretic

https://doi.org/10.1021/acsomega.1c00977
ACS Omega 2021, 6, 13728−13741

migration of the reinforcing phase to the growing metal deposit. Therefore, the preparation involves the following steps: (1) formation of the charged ions; (2) physical movement of the reinforcing phase to the electrode area due to agitation; (3) mass transportation of the reinforcing phase through the diffusion layer; (4) movement of the reinforcing phase due to the potential gradient, and (5) physical embedding of the reinforcing phase into the growing coating.[57] Accordingly, the co-deposition depends on many process parameters, such as current density, electrolyte, temperature, pH value, and the concentration of the reinforcing phase. Figure S1b illustrates the schematic diagram of the co-electrodeposition process.

In the present work, an acidic solution was used, and the experimental parameters are listed in Table 1. As main salts, nickel sulfate ($NiSO_4$) and zinc chloride ($ZnCl_2$) provided zinc ions and nickel ions. Sodium dodecyl sulfate (SDS) was a kind of wetting agent, which not only reduced the surface tension between the electrolyte and coating but also removed the hydrogen bubbles produced during reaction and avoided formation of pinholes on the coating surface.[58] The influence of the SDS surfactant on the deposition behavior of coatings was investigated by many research studies. They demonstrated that good dispersion and uniform distribution of the reinforcement phase in the coatings were achieved when the SDS concentration was increased in the electrolyte. In addition, the SDS was responsible for higher microhardness and better corrosion resistance of the coatings.[23]

Before electrodeposition, the surface of the cathode iron plate (3 cm × 1 cm) was pretreated as follows, that is, first, grinding with SiC paper (from 400# to 1500#) and polishing with Al_2O_3 powder and then ultrasonically cleaning in ethyl alcohol for 5 min, immersing in HCl solution (20%) for 30 s, and at last washing with distilled water. The GO concentrations in the electrolyte varied from 0, 0.2, 0.4, 0.6 to 0.8 g/L while the other components retained the same values. The pH value of the electrolyte was about 3.5−4. The temperature was controlled at 40 °C. The GO aqueous solution was ultrasonically dispersed for 1 h before electrodeposition and meanwhile, the magnetic stirring bath ensured the dispersion of GO during electroplating, as shown in Figure S1c. For comparison, the pure Zn and regular Zn−Ni alloy coatings without Gr were also prepared under the same conditions.

The morphologies and chemical compositions of the samples were characterized by using scanning electron microscopes (S-4800, Hitachi, Japan, and SIRON, FEI, The Netherlands) equipped with EDS. The crystal phases were identified by using an X-ray diffraction spectrometer (D8 ADVANCE, Bruker AXS, Germany) with Cu Kα radiation. The Raman spectra were measured by using a laser scanning confocal micro-Raman spectrometer (LabRAM HR, HORIBA, France) with a laser excitation wavelength of 488 nm and scan on an extended range of 1000−3000 cm^{-1}. The FT-IR spectra were obtained by a Fourier transform infrared spectrometer (Nicolet iS10, Thermo Fisher, USA) over a wavenumber range of 500−4000 cm^{-1}. The hardness and elastic modulus of the samples were tested by using an instrumental nanoindenter (Agilent G200 Nanoindenter, Agilent Technologies, USA) with the continuous stiffness measurement standard programs in which the harmonic depth and frequency were 2 nm and 45 Hz, respectively.

The electrochemical properties of the samples were analyzed by using a CHI electrochemical workstation (CHI760E, Shanghai Chenhua Instruments, Inc., Shanghai, China). A conventional three-electrode cell was used for the electrochemical measurements. 1 cm^2 area of the coated substrate, a platinum sheet, and a saturated calomel electrode (SCE) acted as the working electrode, counter electrode, and reference electrode, respectively. 3.5 wt % NaCl solution was used as the corrosive solution. The open-circuit potential (E_{ocp}) was monitored in order to get a stable potential before corrosion tests. The EIS measurements were taken in a frequency range of 10^5 to 10^{-2} Hz at the E_{ocp} with the employed amplitude of voltage of 10 mV. The potentiodynamic polarization curves were obtained from a cathodic potential of −0.2 mV to an anodic potential of +0.2 mV with respect to E_{ocp} at a scanning speed of 0.5 mV/s.

The adhesion strength between the coating and the substrate was measured according to the scratch tape test standard (ASTM D3359).[59] The experimental steps were as follows: (1) a grid pattern with either six or eleven cuts in each direction was made in the coating to the substrate; (2) a pressure-sensitive tape was applied over the grid and then removed; (3) the adhesion strength was evaluated by comparison with descriptions and illustrations. The weight loss experiment of the samples was carried out in accordance with the standard of ASTM A90/A90M[60] by using a precision electronic balance (FA2004, Shanghai Shunyu Hengping Scientific Instrument Co., Ltd., Shanghai, China).

■ ASSOCIATED CONTENT

Supporting Information

The Supporting Information is available free of charge at https://pubs.acs.org/doi/10.1021/acsomega.1c00977.

Process for preparing the Gr-reinforced Zn−Ni alloy composite coating, including schematic shape of the PRED process and image of electrolytes for electrodeposition, weight loss profiles of the coatings after immersing in 3.5% NaCl solution for 30 days, the surface topography of the composite coating by white light interferometry three-dimensional profiler, and relative texture coefficient for the δ-($Zn_{22}Ni_3$) phase of the composite coating (PDF)

■ AUTHOR INFORMATION

Corresponding Authors

Yupeng Zhang − *Institute of Microscale Optoelectronics, Shenzhen Key Laboratory of Flexible Memory Materials and Devices, Shenzhen University, Shenzhen 518000, China;* orcid.org/0000-0003-2351-5579; Email: ypzhang@szu.edu.cn

Chunxu Pan − *School of Physics and Technology, and MOE Key Laboratory of Artificial Micro- and Nano-structures and Center for Electron Microscopy, Wuhan University, Wuhan 430072, China;* orcid.org/0000-0001-9007-8562; Email: cxpan@whu.edu.cn

Authors

Sishi Li − *School of Physics and Technology, and MOE Key Laboratory of Artificial Micro- and Nano-structures, Wuhan University, Wuhan 430072, China*

Gongsheng Song − *School of Physics and Technology, and MOE Key Laboratory of Artificial Micro- and Nano-structures, Wuhan University, Wuhan 430072, China;* orcid.org/0000-0003-0703-832X

Qiang Fu − *Center for Electron Microscopy, Wuhan University, Wuhan 430072, China*

Complete contact information is available at: https://pubs.acs.org/10.1021/acsomega.1c00977

Notes

The authors declare no competing financial interest.

■ ACKNOWLEDGMENTS

This work was supported by the Science and Technology Innovation Commission of Shenzhen (nos. JCYJ20180305125345378 and JCYJ20170303170542173), the National Natural Science Foundation of China (nos. 51702219 and 61975134), the Natural Science Foundation of Guangdong Province (2015A030313591), the Guangdong Basic and Applied Basic Research Foundation (2020B1515020051), the Shenzhen Nanshan District Pilotage Team Program (LHTD20170006), the Suzhou Science and Technology Project (Prospective Application Research Program, no. SYG201740), and the Chinese Universities Scientific Fund.

■ REFERENCES

(1) Li, Q.; Lu, H.; Cui, J.; An, M.; Li, D. Electrodeposition of nanocrystalline zinc on steel for enhanced resistance to corrosive wear. *Surf. Coat. Technol.* **2016**, *304*, 567−573.

(2) Anwar, S.; Zhang, Y.; Khan, F. Electrochemical behaviour and analysis of Zn and Zn-Ni alloy anti-corrosive coatings deposited from citrate baths. *RSC Adv.* **2018**, *8*, 28861−28873.

(3) Beheshti, M.; Ismail, M. C.; Kakooei, S.; Shahrestani, S.; Mohan, G.; Zabihiazadboni, M. Influence of deposition temperature on the corrosion resistance of electrodeposited zinc-nickel alloy coatings. *Materialwiss. Werkstofftech.* **2018**, *49*, 472−482.

(4) Rekha, M. Y.; Nousheen, N.; Samad, R.; Srivastava, C. Microstructural engineering of ZnCr coating by incorporation of graphene oxide and its effect on the corrosion behaviour of the coating. *Surf. Coat. Technol.* **2020**, *403*, 126422.

(5) Oliveira, R. P.; Bertagnolli, D. C.; da Silva, L.; Ferreira, E. A.; Paula, A. S.; da Fonseca, G. S. Effect of Fe and Co co-deposited separately with Zn-Ni by electrodeposition on ASTM A624 steel. *Appl. Surf. Sci.* **2017**, *420*, 53−62.

(6) Tian, G.; Zhang, M.; Zhao, Y.; Li, J.; Wang, H.; Zhang, X.; Yan, H. High Corrosion Protection Performance of a Novel Non-fluorinated Biomimetic Superhydrophobic Zn-Fe Coating with Echinopsis multiplex-like Structure. *ACS Appl. Mater. Interfaces* **2019**, *11*, 38205−38217.

(7) Ibrahim, M. A. M.; Bakdash, R. S. Copper-rich Cu-Zn alloy coatings prepared by electrodeposition from glutamate complex electrolyte: Morphology, structure, microhardness and electrochemical studies. *Surface. Interfac.* **2020**, *18*, 100404.

(8) Wang, S.; Xue, Y.; Ban, C.; Xue, Y.; Taleb, A.; Jin, Y. Fabrication of robust tungsten carbide particles reinforced Co Ni superhydrophobic composite coating by electrochemical deposition. *Surf. Coat. Technol.* **2020**, *385*, 125390.

(9) ShathishKumar, J. S.; Jegan, A. Assessment on the microhardness and corrosion resistance characteristics of Ni-SiC and Ni-MWCNT coatings by pulse reverse electrodeposition technique. *Mater. Res. Express* **2020**, *7*, 055012.

(10) Yasin, G.; Arif, M.; Mehtab, T.; Shakeel, M.; Khan, M. A.; Khan, W. Q. *Metallic Nanocomposite Coatings*, 2020, pp 245−274. DOI: 10.1016/b978-0-12-819359-4.00014-3.

(11) Tabish, M.; Malik, M. U.; Khan, M. A.; Yasin, G.; Asif, H. M.; Anjum, M. J.; Khan, W. Q.; Ibraheem, S.; Nguyen, T. A.; Slimani, Y.; Nazir, M. T. Construction of NiCo/graphene nanocomposite coating with bulges-like morphology for enhanced mechanical properties and corrosion resistance performance. *J. Alloys Compd.* **2021**, *867*, 159138.

(12) Xiang, T.; Zhang, M.; Li, C.; Dong, C.; Yang, L.; Chan, W. CeO 2 modified SiO 2 acted as additive in electrodeposition of Zn-Ni alloy coating with enhanced corrosion resistance. *J. Alloys Compd.* **2018**, *736*, 62−70.

(13) Li, B.; Li, D.; Xia, W.; Zhang, W. Synthesis and characterization of a novel Zn-Ni and Zn-Ni/Si3N4 composite coating by pulse electrodeposition. *Appl. Surf. Sci.* **2018**, *458*, 665−677.

(14) Ghaziof, S.; Gao, W. The effect of pulse electroplating on Zn-Ni alloy and Zn-Ni-Al2O3 composite coatings. *J. Alloys Compd.* **2015**, *622*, 918−924.

(15) Fayomi, O. S. I.; Popoola, A. P. I.; Kanyane, L. R.; Monyai, T. Development of reinforced in-situ anti-corrosion and wear Zn-TiO2/ZnTiB2 coatings on mild steel. *Results Phys.* **2017**, *7*, 644−650.

(16) Pouladi, S.; Shariat, M. H.; Bahrololoom, M. E. Electrodeposition and characterization of Ni-Zn-P and Ni-Zn-P/nano-SiC coatings. *Surf. Coat. Technol.* **2012**, *213*, 33−40.

(17) Luo, H.; Leitch, M.; Behnamian, Y.; Ma, Y.; Zeng, H.; Luo, J.-L. Development of electroless Ni-P/nano-WC composite coatings and investigation on its properties. *Surf. Coat. Technol.* **2015**, *277*, 99−106.

(18) Praveen, B. M.; Venkatesha, T. V. Electrodeposition and properties of Zn-Ni-CNT composite coatings. *J. Alloys Compd.* **2009**, *482*, 53−57.

(19) Song, G.; Li, S.; Liu, G.; Fu, Q.; Pan, C. Influence of Graphene Oxide Content on the Zn-Gr Composite Layer Prepared by Pulse Reverse Electro-plating. *J. Electrochem. Soc.* **2018**, *165*, D501−D510.

(20) Yasin, G.; Anjum, M. J.; Malik, M. U.; Khan, M. A.; Khan, W. Q.; Arif, M.; Mehtab, T.; Nguyen, T. A.; Slimani, Y.; Tabish, M.; Ali, D.; Zuo, Y. Revealing the erosion-corrosion performance of sphere-shaped morphology of nickel matrix nanocomposite strengthened with reduced graphene oxide nanoplatelets. *Diamond Relat. Mater.* **2020**, *104*, 107763.

(21) Yasin, G.; Khan, M. A.; Arif, M.; Shakeel, M.; Hassan, T. M.; Khan, W. Q.; Korai, R. M.; Abbas, Z.; Zuo, Y. Synthesis of spheres-like Ni/graphene nanocomposite as an efficient anti-corrosive coating; effect of graphene content on its morphology and mechanical properties. *J. Alloys Compd.* **2018**, *755*, 79−88.

(22) Yasin, G.; Arif, M.; Shakeel, M.; Dun, Y.; Zuo, Y.; Khan, W. Q.; Tang, Y.; Khan, A.; Nadeem, M. Exploring the Nickel-Graphene Nanocomposite Coatings for Superior Corrosion Resistance: Manipulating the Effect of Deposition Current Density on its Morphology, Mechanical Properties, and Erosion-Corrosion Performance. *Adv. Eng. Mater.* **2018**, *20*, 1701166.

(23) Yasin, G.; Arif, M.; Nizam, M. N.; Shakeel, M.; Khan, M. A.; Khan, W. Q.; Hassan, T. M.; Abbas, Z.; Farahbakhsh, I.; Zuo, Y. Effect of surfactant concentration in electrolyte on the fabrication and properties of nickel-graphene nanocomposite coating synthesized by electrochemical co-deposition. *RSC Adv.* **2018**, *8*, 20039−20047.

(24) Berry, V. Impermeability of graphene and its applications. *Carbon* **2013**, *62*, 1−10.

(25) Song, N.; Chen, D.; Luo, L. L.; Chen, J. R. An Overview with Applications to Graphene-Based Composites. *Appl. Mech. Mater.* **2014**, *556*−*562*, 96−99.

(26) Xiao, H.; Xiaoying, Q.; Boey, F.; Hua, Z. Graphene-based composites. *Chem. Soc. Rev.* **2012**, *41*, 666−686.

(27) Yang, Y.; Song, G.; Fu, Q.; Pan, C. Preparation of Fe - Gr composite layer via DC electro-plating for high performances. *J. Alloys Compd.* **2018**, *768*, 859−865.

(28) Li, F.; Yang, H.; Shan, C.; Zhang, Q.; Han, D.; Ivaska, A.; Niu, L. The synthesis of perylene-coated graphene sheets decorated with Au nanoparticles and its electrocatalysis toward oxygen reduction. *J. Mater. Chem.* **2009**, *19*, 4022.

(29) Zhang, X.; Zhou, Y.; Liang, A.; Zhang, B.; Zhang, J. Facile fabrication and corrosion behavior of iron and iron-reduced graphene oxide composite coatings by electroless plating from baths containing no reducing agent. *Surf. Coat. Technol.* **2016**, *304*, 519−524.

(30) Luo, H.; Sui, Y.; Qi, J.; Meng, Q.; Wei, F.; He, Y. Copper matrix composites enhanced by silver/reduced graphene oxide hybrids. *Mater. Lett.* **2017**, *196*, 354−357.

(31) Leng, J. F.; Teng, X. Y.; Jiang, F. L.; Hu, D. J.; Geng, H. R. Preparation of Graphene and Graphene/Al Composites. *Mater. Sci. Forum* **2015**, *816*, 177−181.
(32) Jabbar, A.; Yasin, G.; Khan, W. Q.; Anwar, M. Y.; Korai, R. M.; Nizam, M. N.; Muhyodin, G. Electrochemical deposition of nickel graphene composite coatings: effect of deposition temperature on its surface morphology and corrosion resistance. *RSC Adv.* **2017**, *7*, 31100−31109.
(33) Li, S.; Song, G.; Fu, Q.; Pan, C. Preparation of Cu- graphene coating via electroless plating for high mechanical property and corrosive resistance. *J. Alloys Compd.* **2019**, *777*, 877−885.
(34) Li, W.; Li, D.; Fu, Q.; Pan, C. Conductive enhancement of copper/graphene composites based on high-quality graphene. *RSC Adv.* **2015**, *5*, 80428−80433.
(35) Dreyer, D. R.; Park, S.; Bielawski, C. W.; Ruoff, R. S. The chemistry of graphene oxide. *Chem. Soc. Rev.* **2010**, *39*, 228−240.
(36) Song, G.; Sun, L.; Li, S.; Sun, Y.; Fu, Q.; Pan, C. Synergistic effect of Gr and CNTs on preparing ultrathin Cu-(CNTs+Gr) composite foil via electrodeposition. *Composites, Part B* **2020**, *187*, 107841.
(37) Wu, H.; Liu, F.; Gong, W.; Ye, F.; Hao, L.; Jiang, J.; Han, S. Preparation of Ni-P-GO composite coatings and its mechanical properties. *Surf. Coat. Technol.* **2015**, *272*, 25−32.
(38) Wasekar, N. P.; Jyothirmayi, A.; Hebalkar, N.; Sundararajan, G. Influence of pulsed current on the aqueous corrosion resistance of electrodeposited zinc. *Surf. Coat. Technol.* **2015**, *272*, 373−379.
(39) Moshgi Asl, S.; Afshar, A.; Yaghoubinezhad, Y. An Electrochemical Synthesis of Reduced Graphene Oxide/Zinc Nanocomposite Coating through Pulse-Potential Electrodeposition Technique and the Consequent Corrosion Resistance. *Int. J. Corros.* **2018**, *2018*, 1−13.
(40) Rattana; Chaiyakun, S.; Witit-anun, N.; Nuntawong, N.; Chindaudom, P.; Oaew, S.; Kedkeaw, C.; Limsuwan, P. Preparation and characterization of graphene oxide nanosheets. *Procedia Eng.* **2012**, *32*, 759−764.
(41) Ni, Z.; Wang, Y.; Yu, T.; Shen, Z. Raman spectroscopy and imaging of graphene. *Nano Res.* **2008**, *1*, 273−291.
(42) Kumar, N. A.; Choi, H.-J.; Shin, Y. R.; Chang, D. W.; Dai, L.; Baek, J.-B. Polyaniline-Grafted Reduced Graphene Oxide for Efficient Electrochemical Supercapacitors. *ACS Nano* **2012**, *6*, 1715−1723.
(43) Pavithra, C. L.; Sarada, B. V.; Rajulapati, K. V.; Rao, T. N.; Sundararajan, G. A new electrochemical approach for the synthesis of copper-graphene nanocomposite foils with high hardness. *Sci. Rep.* **2014**, *4*, 4049.
(44) Zhou, M.; Wang, Y.; Zhai, Y.; Zhai, J.; Ren, W.; Wang, F.; Dong, S. Controlled synthesis of large-area and patterned electrochemically reduced graphene oxide films. *Chemistry* **2009**, *15*, 6116−6120.
(45) Song, G.; Yang, Y.; Fu, Q.; Pan, C. Preparation of Cu-Graphene Composite Thin Foils via DC Electro-Deposition and Its Optimal Conditions for Highest Properties. *J. Electrochem. Soc.* **2017**, *164*, D652−D659.
(46) Du, G.; Wang, X.; Zhang, L.; Feng, Y.; Liu, Y. One-step green synthesis of graphene-ZnO nanocomposites. *Mater. Lett.* **2013**, *98*, 168−170.
(47) Wang, P.; Li, T.; Zhang, D. Fabrication of non-wetting surfaces on zinc surface as corrosion barrier. *Corros. Sci.* **2017**, *128*, 110−119.
(48) Li, R.; Liang, J.; Hou, Y.; Chu, Q. Enhanced corrosion performance of Zn coating by incorporating graphene oxide electrodeposited from deep eutectic solvent. *RSC Adv.* **2015**, *5*, 60698−60707.
(49) Raghupathy, Y.; Kamboj, A.; Rekha, M. Y.; Narasimha Rao, N. P.; Srivastava, C. Copper-graphene oxide composite coatings for corrosion protection of mild steel in 3.5% NaCl. *Thin Solid Films* **2017**, *636*, 107−115.
(50) Mišković-Stanković, V.; Jevremović, I.; Jung, I.; Rhee, K. Electrochemical study of corrosion behavior of graphene coatings on copper and aluminum in a chloride solution. *Carbon* **2014**, *75*, 335−344.
(51) Naghdi, S.; Nešović, K.; Mišković-Stanković, V.; Rhee, K. Y. Comprehensive electrochemical study on corrosion performance of graphene coatings deposited by chemical vapour deposition at atmospheric pressure on platinum-coated molybdenum foil. *Corros. Sci.* **2018**, *130*, 31−44.
(52) Raghupathy, Y.; Natarajan, K. A.; Srivastava, C. Anti-corrosive and anti-microbial properties of nanocrystalline Ni-Ag coatings. *Mater. Sci. Eng. B* **2016**, *206*, 1−8.
(53) Wei, T.; Fa-qin, X.; Xiang-qing, W. Corrosion Resistance of Electroplating Zinc-Nickel Alloy. *Corros. Prot.* **2006**, *27*, 552−554.
(54) Kirkland, N. T.; Schiller, T.; Medhekar, N.; Birbilis, N. Exploring graphene as a corrosion protection barrier. *Corros. Sci.* **2012**, *56*, 1−4.
(55) Lu, W. Synthesis and Characterization of Graphene Oxide with Improved Hummers Method. *Packag. J.* **2015**, *7*, 28−31.
(56) Chandrasekar, M. S.; Pushpavanam, M. Pulse and pulse reverse plating-Conceptual, advantages and applications. *Electrochim. Acta* **2008**, *53*, 3313−3322.
(57) Walsh, F. C.; Ponce de Leon, C. A review of the electrodeposition of metal matrix composite coatings by inclusion of particles in a metal layer: an established and diversifying technology. *Trans. IMF* **2014**, *92*, 83−98.
(58) Zhouqin, L.; Guangang, C.; Zhenquan, L.; Peichang, W. Dodocyl sulfate sodium salt is an excellent reagent which inhibits pinholes in plating nickel layer. *Plat. Coat.* **2018**, *11*, 36−39.
(59) *Standard Test Methods for Measuring Adhesion by Tape Test*; ASTM International: West Conshohocken, 2008; Vol. *D 3359-08*.
(60) *Standard Test Method for Weight [Mass] of Coating on Iron and Steel Articles with Zinc or Zinc-Alloy Coatings*; ASTM International: West Conshohocken, 2018; Vol. *A90/A90M*.

https://doi.org/10.1021/acsomega.1c00977
ACS Omega 2021, 6, 13728−13741